RSC Advances

This article can be cited before page numbers have been issued, to do this please use: Y. Liu, S. yao, Q. Yang, P. Sun, Y. Gao, X. Liang, F. Liu and G. lu, *RSC Adv.*, 2015, DOI: 10.1039/C5RA07213A.

ROYAL SOCIETY OF CHEMISTRY

www.rsc.org/advances

View Article Online
DOI: 10.1039/C5RA07213A

Rsc advances

ARTICLE

Highly sensitive and humidity-independent ethanol sensors based on In_2O_3 nanoflower/SnO_2 nanoparticle composites

Received 00th January 20xx,
Accepted 00th January 20xx

DOI: 10.1039/x0xx00000x

www.rsc.org/

Yang Liu[a], Shiting Yao[a], Qiuyue Yang[a], Peng Sun[a], Yuan Gao*[a], Xishuang Liang[a], Fengmin Liu*[a] and Geyu Lu[a]

Abstract

As an ethanol sensing material, the composites In_2O_3-SnO_2 were composed of In_2O_3 microflowers and SnO_2 nanoparticles. Both In_2O_3 microflowers and SnO_2 nanoparticles were synthesized by hydrothermal method and then mixed under ultrasonic environment. The morphology and phase composition of the as-synthesized samples were characterized by X-ray powder diffraction (XRD) and scanning electron microscopy (SEM). The results on gas sensing properties showed that while the mass ratio of In_2O_3 and SnO_2 was 2:1, the sensors based on as-prepared In_2O_3-SnO_2 composites exhibited high response and good selectivity to ethanol at 250℃.The response to 100 ppm ethanol gas was 53.2. UV illumination stabilized response of the sensors while the relative humidity increased. The gas sensing mechanism was that proposed the addition of SnO_2 to In_2O_3 enhanced the catalytic activity for the ethanol reaction, which changed the electrical resistance of the materials. Besides, the morphology was helpful to the gas reaction on the surface of the sensing materials.

1.Introduction

The ethanol detection on the breath is an effective way to aid police in apprehending drink driving offenders[1]. In addition, as a kind of volatile organic compounds (VOCs), the ethanol detection can potentially be utilized as breath markers for specific diseases[2].Thus far, several types of ethanol sensors have been reported for breath analysis[3,4,5]. In recent years, the semiconductor gas sensors have attracted widespread concern to science researchers because of their high sensitivity, low cost and simplicity [6.7,8]. It is well known that the performances of sensors are significantly influenced by the component, crystalline size and morphology of sensing materials[9,10,11].

Generally, the smaller crystal size owns bigger surface area, which provides more active sites for the target gas reacting with the sensing materials. However, agglomeration of fine particles greatly reduces the valid surface area. Fortunately, hierarchical nanostructure oxides emerged due to their high active surface area and loose microstructure favourable for gas adsorption and rapid gas diffusion, and have dominated the research in enhancing the sensitivity of the metal oxide gas sensors. Another important sensing parameter is selectivity that can be improved through the use of composite metal oxides[12,13,14]. The physical interface between two dissimilar materials is often referred to as a heterojunction. In Akbar et al [15] review, the authors detailed the dominant electronic and chemical mechanisms that influence the performance of the metal oxide heterojunction as resistive-type gas sensors.

Up to date, many composites such as In_2O_3-CeO_2, ZnO-SnO_2, TiO_2-SnO_2, SnO_2-Fe_2O_3 [16,17,18,19] have been reported to be promising sensing materials to obtain the sensitive and selective gas sensors. As two important kinds of fundamental materials, In_2O_3 and SnO_2 have been widely studied due to their responses towards different gases [20,21,22,23]. In_2O_3-SnO_2 composites [24,25] have also been proved to improve the properties of sensors. However, to the best of our knowledge, there are few reports on the morphology of In_2O_3-SnO_2 composites and no reports have shown that In_2O_3-SnO_2 composites have an excellent response and selectivity for ethanol.

Commonly, the water vapour strongly interacts with the oxide semiconductor surface, which leads to a significant deterioration of the sensor performance. There is high humidity in breath, so it is very important to reduce the influence of humidity on the performance of the sensors.

[a]State Key Laboratory on Integrated Optoelectronics, College of Electronic Science and Engineering, Jilin University, 2699 Qianjin Street, Changchun 130012, People's Republic of China. E-mail: 18946580425@163.com, liufm@jlu.edu.cn;Fax: +86-431-85167808;Tel:0431-85168384.

† Electronic Supplementary Information (ESI) available:. Details of preparations and characterizations; the SEM images using a JEOL JSM-7500F microscope with an accelerating voltage of 15 kV; the XRD measurements with a Rigaku D/max-2500 diffractometer using Cu-Kα1 radiation; the BET measurements with a Micromeritics Gemini VII apparatus (Surface Area and Porosity System);
See DOI: 10.1039/x0xx00000x

View Article Online
DOI: 10.1039/C5RA07213A

In this work, In_2O_3 microflowers and SnO_2 nanoparticles were both synthesized by hydrothermal method. Then the two kinds of materials were mixed in the ultrasound environment. The testing on gas sensing properties showed that while the mass ratio of In_2O_3 and SnO_2 was 2:1, the sensors based on In_2O_3-SnO_2 composite oxides showed the highest response to ethanol, the response to 100ppm ethanol gas was 53.2 at 250 ℃.UV illumination was adopted to reduce the influence of relative humidity on the performances of the sensors.

2. Experimental

2.1 Synthesis and characterization of the samples

In_2O_3 was synthesized according to the literatures[26].In a typical synthesis process,0.381 g of $In(NO_3)_3$•$4.5H_2O$ and 0.15 g urea were dissolved in 36 mL deionized water with stirring until the solution was clear. Then, the mixture solution was transferred into a Teflon-lined stainless steel autoclave, heated at 160℃ for 4 h. After the autoclave was cooled to room temperature naturally, the result product was washed with deionized water and ethanol for six times alternately by centrifuge, and then dried at 80℃ for 3 h. The products were sintered to 500℃ at a rate of 2℃/min and then kept at 500℃ for 2 h. Then In_2O_3 microflowers were synthesized.

SnO_2 was synthesized according to the literatures[27].In a typical synthesis process,0.526 g of $SnCl_4$•$5H_2O$, 0.6 g of cetyltrimethyl ammonium bromide (CTAB) and 0.2 g of hexamethylenetetramine (HMT) were added to 40 mL mixed solvent of ethanol and water (1:1, v/v) with stirring until the solution was clear. Then, the mixture solution was transferred into a Teflon-lined stainless steel autoclave, heated at 200℃ for 4 h.The processes after this were same with the process used to synthesize In_2O_3.

Then In_2O_3 microflowers and SnO_2 nanoparticles were mixed physically in certain mass ratio under ultrasound environment. Four In_2O_3-SnO_2 composites samples with mass concentration of 0% SnO_2, 33.3% SnO_2, 70% SnO_2 and 100% SnO_2 were obtained, represented by S0, S1, S2 and S3, respectively. Until this step, In_2O_3-SnO_2 composites were obtained.

2.2 Fabrication and measurement of sensors

Gas sensors were fabricated as follows: the prepared materials (S0, S1, S2 and S3) were mixed with deionized water to form something like slurry, and then spread on an alumina tube (4 mm in length, 1.2 mm in external diameter, and 0.8 mm in internal diameter, attached with a pair of gold electrodes, each electrode was connected with two Pt wire)by a small brush until forming a film thick enough to cover the gold electrode entirely. A Ni-Cr heating wire went through the tube to support heat for the sensors. The resistances of the sensors were measured by multimeter (fluke 8846A) under constant temperature and humidity. The measurement was processed by a static test system: R_a and R_g were the resistances of the sensors in air and tested gas, respectively. A certain amount of the tested gas was injected into a closed chamber, and the sensor was put into the chamber for the measurement of the sensitive performance. When the response reached a constant value, the sensor was removed to air to recover. The response of the sensor was defined as $S=R_a/R_g$ for reducing gases or R_g/R_a for oxidizing gases. The response and recovery times are defined as the times taken by the resistance change of sensor achieving 90% of the total in the case of adsorption and desorption, respectively.

UV illumination was processed according our previous works[28,29]. UV-LED (peak wavelength= 380 nm; operating voltage =3 V) was chosen as the light source, and the distance between the UV-LED and gas sensors was 2 mm. The measured power of the UV-LED at this distance was 0.7 Cd/m^2 (PR650, California, USA).Relative humidity (%RH) was obtained by using Humidity generator (Shanghai ESPEC environmental equipment corp.SETH-Z-022L).

In order to investigate the repeatability of the sensors .The fabrication and measurement of sensors were repeated 5 times, the results showed the sensors had similar properties.

3. Results and discussion

3.1 Characterization of the products

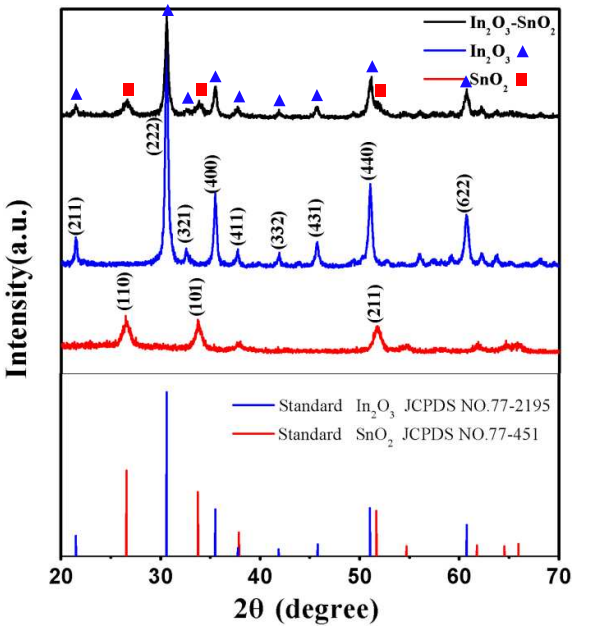

Fig.1 XRD of In_2O_3 microflowers, SnO_2 nanoparticles and In_2O_3-SnO_2 composites.

View Article Online
DOI: 10.1039/C5RA07213A

The crystal phase of In_2O_3 microflowers, SnO_2 nanoparticles and In_2O_3-SnO_2 composites were investigated by XRD with a Rigaku D/max-2500 diffractometer using Cu-Kα1 radiation. From the Fig.1, we can see that In_2O_3-SnO_2 composites has all peaks of In_2O_3 and SnO_2.They were in good agreement with the JCPDS file of In_2O_3 (JCPDS NO.71-2195) and SnO_2 (JCPDS NO.77-451).It proved that In_2O_3 microflowers and SnO_2 nanoparticles were mixed entirely by physical route and they had no chemical reacts. No diffraction peaks from any other impurities were observed, indicating the high purity of the products.

3.2 Structural and morphological characteristics

The morphologies and structures of In_2O_3 microflowers, SnO_2 nanoparticles and In_2O_3-SnO_2 composites were identified by SEM using a JEOL JSM-7500F microscope with an accelerating voltage of 15 kV as shown in Fig.2. Fig.2 (a) presents the SEM image of SnO_2 particles, it can be seen that SnO_2 particles are composed of relatively uniform SnO_2 nanoparticles with a length of 20-30 nm. It can be seen that the surfaces of nanoparticles are coarse. As is shown in Fig.2 (b), the In_2O_3 microflowers have a good dispersion and uniform size of 1-1.5 μm, it can be seen from the image that the In_2O_3 microflowers are composed of aggregated nanosheets.Fig.2 (c) shows In_2O_3-SnO_2 composites, SnO_2 nanoparticles seems to be surrounded by In_2O_3 microflowers, SnO_2 and In_2O_3 was marked with boxes. Composition of In_2O_3-SnO_2 composites had been characterized using EDS as shown in Fig.2 (d). The EDS spectrum showed that components of the materials are In, Sn and O. The Si was attributed to the substrate used in the SEM measurement.

Fig.3 shows nitrogen adsorption-desorption isotherm and pore size distribution (inset of Fig. 3) of the In_2O_3 microflowers, SnO_2 nanoparticles and In_2O_3-SnO_2 composites. Pore size distribution curves were calculated from the desorption branch of a nitrogen isotherm by the BJH method using the Halsey equation. The BET surface area of the In_2O_3 microflowers, SnO_2 nanoparticles and In_2O_3-SnO_2 composites were calculated to be 19.5 m^2/g, 41.0 m^2/g and 34.4 m^2/g respectively by the Brunauer-Emmett-Teller (BET) method with a Micromeritics Gemini VII apparatus (Surface Area and Porosity System).

3.3 Gas-sensing properties

As we know, the mass ratio of In_2O_3 microflowers and SnO_2 nanoparticles and the working temperature both influenced greatly gas responses in this research, so the gas sensing properties of S0 to S3 to 100 ppm ethanol under different temperatures were investigated, the results were shown in Fig.4.The VOCs were got from liquid evaporation, concentration calculation method is according to ideal gas

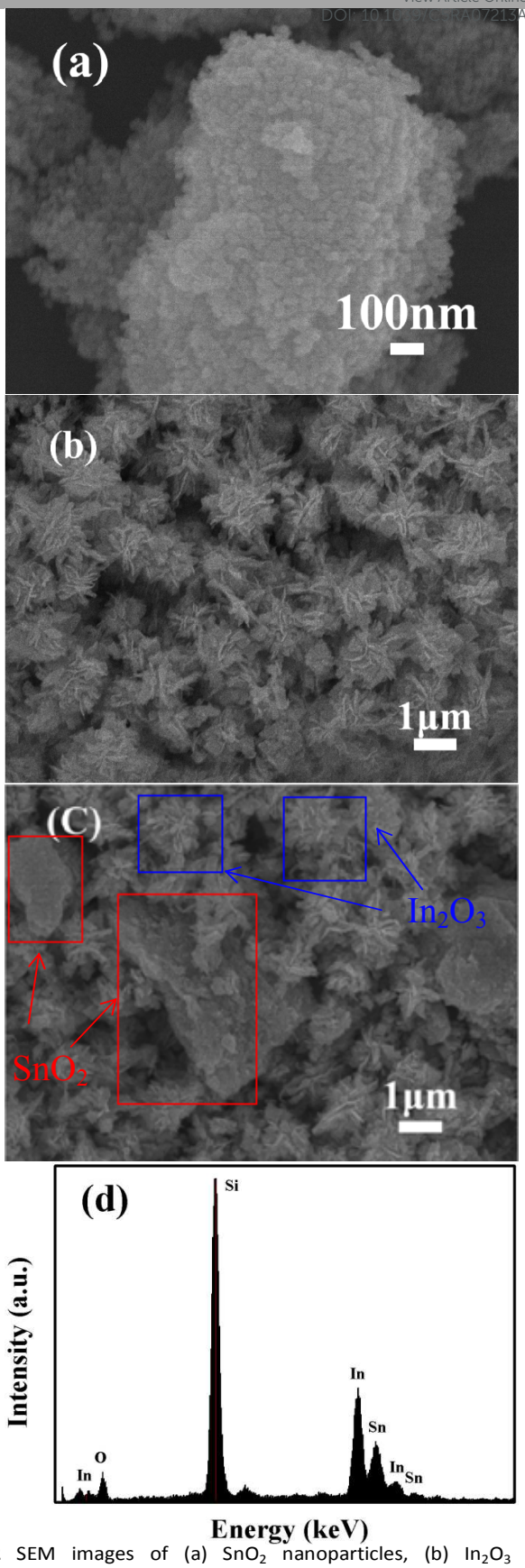

Fig.2 SEM images of (a) SnO_2 nanoparticles, (b) In_2O_3 microflowers and (c) In_2O_3-SnO_2 composites (d) EDS spectra of In_2O_3-SnO_2 composites.

View Article Online
DOI: 10.1039/C5RA07213A

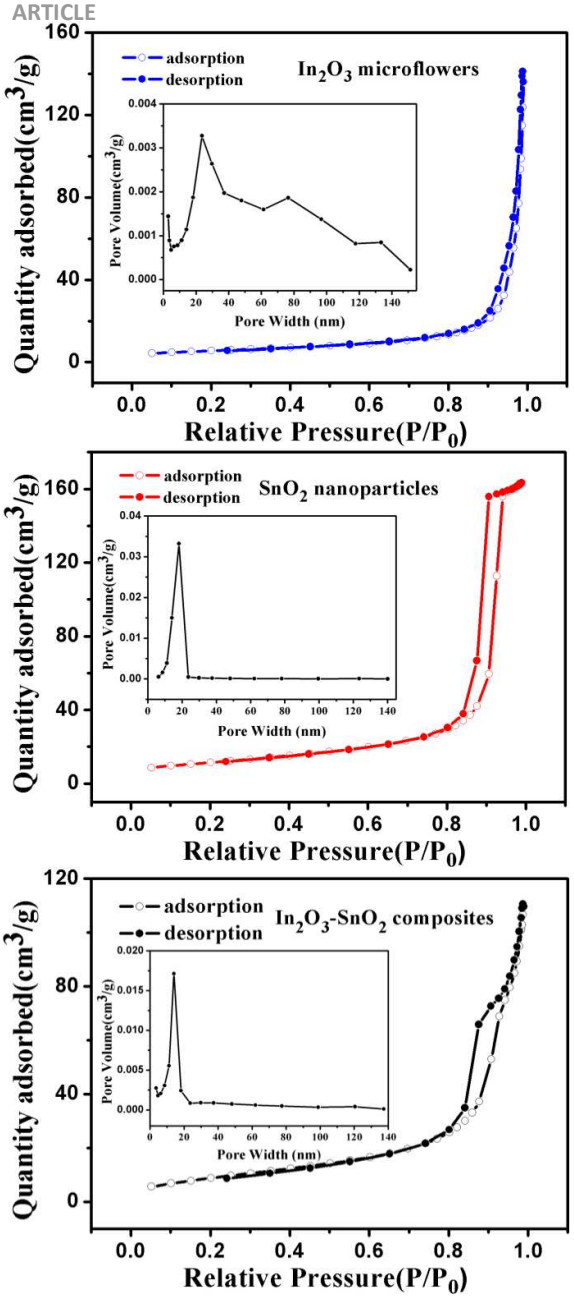

Fig.3 Typical N_2 adsorption-desorption isotherms and pore size distribution of In_2O_3 microflowers, SnO_2 nanoparticles and In_2O_3-SnO_2 composites.

equation of state (PV=nRT).The sensors based the In_2O_3-SnO_2 composites (S1) showed the best response while the mass ratio of In_2O_3 and SnO_2 was 2:1.The best response to 100 ppm ethanol was 53.2 at 250℃. A comparison between the sensing performances of the sensor and literature reports[26,27,30,31,32] were summarized in Table 1.

Fig.5 shows the responses of the sensors based on S1 to different concentrations ethanol at 250℃.Before 500 ppm, the responses increase with the ethanol concentration like a line, when the ethanol concentration is more than 500 ppm,

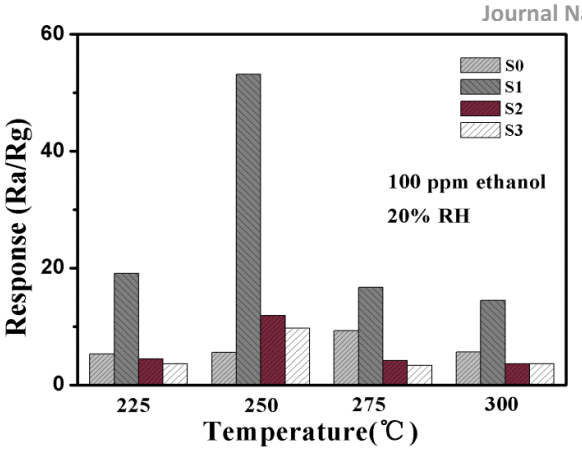

Fig.4 Responses of sensors based on S0-S3 to 100 ppm ethanol.

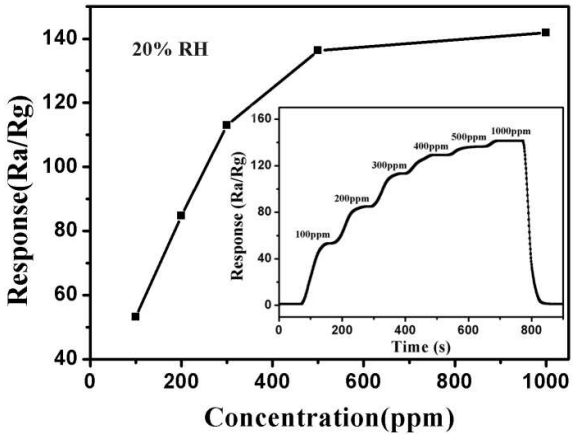

Fig.5 Relationship between responses of sensors based on S1 and ethanol concentration at 250℃, the inset displaying dynamic response.

the response is nearly saturated. Dynamic response towards 100-1000 ppm ethanol at 250℃ was shown in the inset of Fig.5.

The response and recovery characteristics were investigated which were shown in the Fig.6 (a).The results indicate that the In_2O_3-SnO_2 composites sensor based on S1 has fast response-recovery kinetics. The response and recovery times of the In_2O_3-SnO_2 composites sensors are about 15 s and 60 s, respectively. Five reversible cycles of the response curve indicate a stable and repeatable characteristic, as shown in Fig.6 (b).

Selectivity is also an important performance of the sensor based on the as-prepared In_2O_3-SnO_2 composites to various gases, such as NO, H_2S, NO_2, $C_6H_5CH_3$, C_3H_6O, CH_3OH, HCHO and CH_3CH_2OH.All of the gases were tested at an operating temperature of 250℃ as shown in Fig.7. The response of the sensors based on In_2O_3-SnO_2 composites (S1) to toluene, acetone and methanol is much lower than ethanol, and the response to other gases or vapours such as NO, H_2S, NO_2 and formaldehyde is negligible. The results indicate that the as-prepared In_2O_3-SnO_2 composites display superior

View Article Online
DOI: 10.1039/C5RA07213A

Table 1

Material	Fabrication approach	Ethanol concentration(ppm)	Temperature (℃)	Sensor response	Reference
In_2O_3microflowers	Hydrothermal route	100ppm	RT	~1.5	[26]
SnO_2 nanostructures	Hydrothermal route	100ppm	275℃	~9.6	[27]
SnO_2–In_2O_3	Sol-gel and electrospinning	100ppm	RT	~3.0	[30]
In_2O_3 nanospheres	Hydrothermal route	100ppm	275℃	~21.0	[31]
In_2O_3-SnO_2 nanocomposites	Mechanochemical reaction	100ppm	RT	~18.7	[32]
In_2O_3-SnO_2 composites	Hydrothermal route	100ppm	250℃	53.2	This work

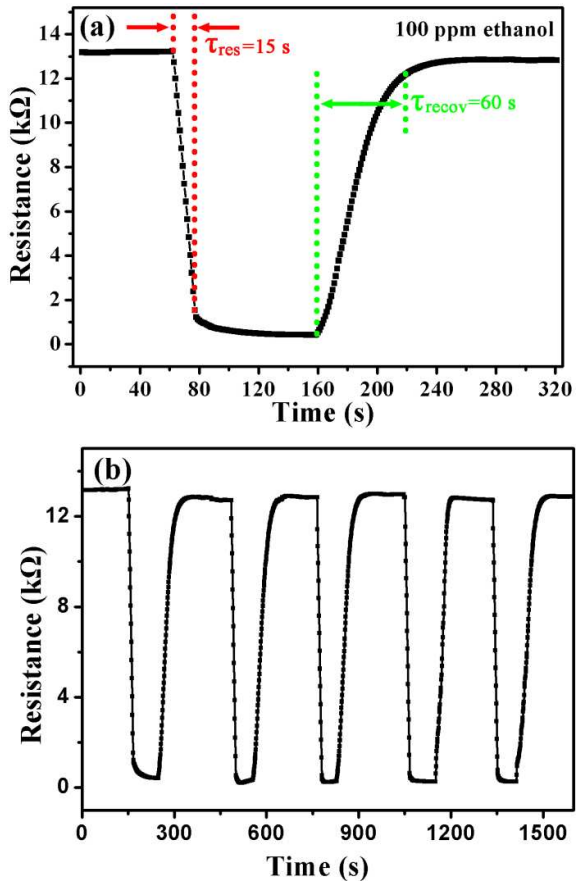

Fig.6 (a) Dynamic response resistance of the sensor (S1) and (b) five periods of response curve of the sensor to 100 ppm ethanol at 250℃ (20%RH).

selectivity to ethanol against the other interference gases and was very suitable for sensing ethanol at 250℃.

UV illumination was used to enhance the performance of the sensors (S1). Although the sensitivity and the response and recovery times were almost not affected by UV illumination, UV illumination greatly reduced the influence of humidity on the sensitivity of the sensors, the results were shown in Fig.8. It can be seen that the sensitivity is almost stable below 80% RH under UV illumination. When the relative humidity is even up to 95%RH, the sensitivity still maintains 75%, which is higher than that without UV illumination. UV illumination can decompose the water vapour on the surface according to the mechanism of photochemical water splitting (Water can be decomposed into hydrogen and oxygen under UV illumination[33]).

3.4 Gas mechanism

The formation of metal oxide composites is known to increase the response and selectivity to gases. For this work,

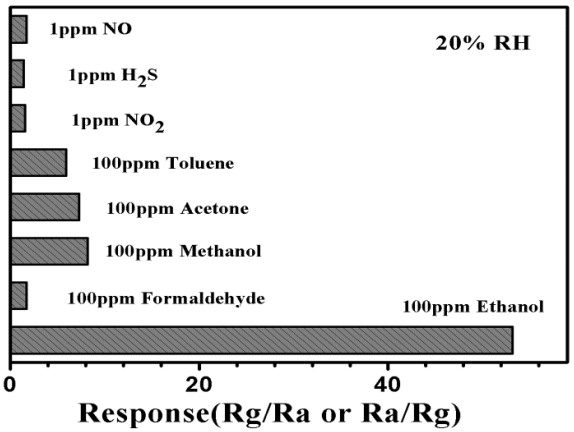

Fig.7 Comparison of responses of In_2O_3-SnO_2 composites (S1) sensors to various gases at 250℃.

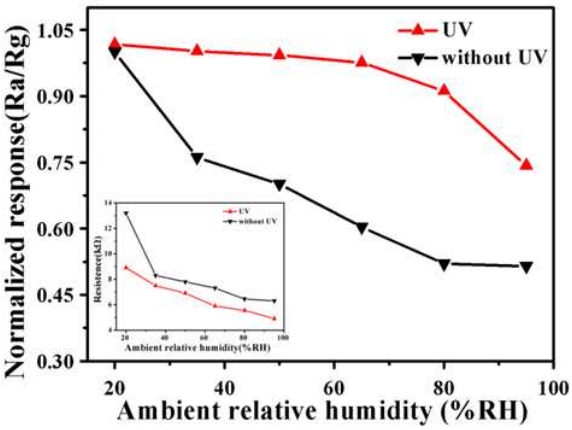

Fig. 8 Responses of the sensors (S1) in different relative humidity, the inset is the resistances in air vs relative humidity.

View Article Online
DOI: 10.1039/C5RA07213A

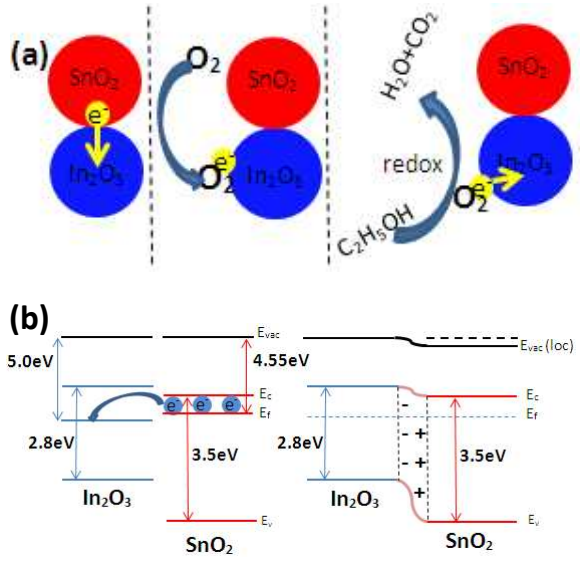

Fig.9 (a) Schematic diagram of the proposed mechanism of In_2O_3-SnO_2 composites and (b) Energy band structure of In_2O_3, SnO_2 and In_2O_3–SnO_2 composites.

both In_2O_3 and SnO_2 increase the response and selectivity to gases. For this work, both In_2O_3 and SnO_2 are n-type semiconductor oxides. The surface of the sensor material in air is covered with chemisorbed oxygen ions such as O^-, O^{2-} and O_2^{2-}, the electrons on chemisorbed oxygen ions come from the material, which decrease the electron density in n-type material and in turn increase the resistance of the oxide. If reducing gas is introduced, it reacts with the surface adsorbed oxygen, the electron will be donated back into the semiconductor that causes a decrease in the resistance. Adsorbed ethanol undergoes two possible mechanisms of dehydrogenation to an aldehyde and dehydration to an alkene, shown in reactions (1) and (2)[34].

$$C_2H_5OH\ (g) \rightarrow CH_3CHO\ (g) + H_2\ (g) \quad (1)$$

$$C_2H_5OH\ (g) \rightarrow C_2H_4\ (g) + H_2O\ (g) \quad (2)$$

Following this process consecutive reactions happen which consume ionic oxygen species and release electrons, so the resistance of the oxide is reduced. The electrons only removed to a certain depth from the surface known as the depletion region. The depletion region width may change as the test gas or oxygen is adsorbed on the surface, which in turn caused a measurable change in the resistance. This process was shown in Fig.9 (a).

The enhancement in gas-sensing property on In_2O_3 and SnO_2 composites may be mainly ascribed to heterostructure [35,36]. The SnO_2 has a lower Fermi level than that of In_2O_3, In_2O_3 would receive electrons from SnO_2, leading to the formation of an accumulation layer at the In_2O_3-SnO_2 interface, as shown in Fig.9 (b). The increase of electrons on the surface of In_2O_3 is in favour of adsorption of O_2 and decrease of resistance.

Besides, In_2O_3 and SnO_2 were both active site, but each promoted different breakdown profiles of the ethanol vapours being sensed. Because of their complementary catalytic activity (catalytic activity reaches an optimum level when the mass ratio of In_2O_3 and SnO_2 is 2:1), the mixed oxides permitted a more complete breakdown of the ethanol vapours, leading to the observed enhancement in sensitivity. In addition, the porous structure is helpful for gas diffusion and its reaction on the surface of the sensing materials.

4. Conclusions

In summary, In_2O_3-SnO_2 composites had been successfully obtained through a mixing of In_2O_3 microflowers and SnO_2 nanoparticles. The nanostructure is in favour of permeation of the tested gas. The In_2O_3-SnO_2 sensors exhibit high response and good selectivity to ethanol at 250℃. It can detect 100ppm ethanol with a response value of about 53.2 and with little interference from other gases. The enhancement in gas-sensing property on In_2O_3 and SnO_2 composites may be ascribed to heterostructure. Because of the depletion layer manipulation and complementary catalytic activity, the composite oxides permitted a more complete breakdown of the ethanol vapours, leading to the observed enhancement in sensitivity and selectivity. The sensitivity is stable while the relative humidity increasing under UV illumination due to photochemical water splitting.

Acknowledgments

This work is supported by the National Nature Science Foundation of China (Nos. 61074172, 61134010, and 61327804) and Program for Chang Jiang Scholars and Innovative Research Team in University (No. IRT1017). National High-Tech Research and Development Program of China (863 Program, No. 2013AA030902).

Notes and references

1 S. K., Chimia, 2002, 56, 59-62.
2 M. Seo, M. Yuasa and T. Kida, J. Ceram. Soc. Jpn., 2011, 119, 884-889.
3 K. Tetsuya, H. Hiroaki and M. Takuya etc, J. Phys. Chem. C., 2010, 114, 15141-15148.
4 J. Wang and M. Musameh, Anal. Chem., 2003, 75, 2075-2079.
5 M. Penza, F. Antolini and M. Vittori-Antisari, Thin Solid Films, 2005,472, 246-252.
6 P. Sun, X. He, W. Wang, J. Ma, Y. Sun and G. Lu, Crystengcomm, 2012, 14, 2229-2234.
7 C. Wang, X. Cheng, X. Zhou, P. Sun , X. Hu, K. Shimanoe, G. Lu and N. Yamazoe, ACS Appl. Mat. Interfaces 2014, 6, 12031-12037.

View Article Online
DOI: 10.1039/C5RA07213A

8 P. Sun, X. Zhou, C. Wang, K. Shimanoe, G. Lu and N. Yamazoe, J. Mater. Chem. A, 2014, 2, 1302–1308.
9 Y. Guan, D. Wang, X. Zhou, P. Sun, H. Wang, J. Ma and G. Lu, Sens. Actuators B, 2014, 191, 45-52.
10 C. Wang, X. Li, B. Wang, J. Ma, Y. Cao, Y. Sun and G. Lu, RSC Adv., 2014, 4, 18365-18369.
11 X. Zhou, C. Wang, W. Feng, P. Sun, X. Li and G. Lu, Mater. Lett., 2014, 120, 5-8.
12 S.I. Rembeza, N.N. Kosheleva and E.S. Rembeza etc, Semiconductors 2014, 48, 1118-1122.
13 J. Susanna, P. Katrin and G. Anton. J etc, Adv. Funct. Mater., 2007, 17, 3339-3347.
14 P. M. Dominic, F. E. P. Keith and T. Paraskeva etc, IEEE Sens. J., 2007, 7, 551-556.
15 D.R. Miller, S. A. Akbar and P. A. Morris, Sens. Actuators B, 2014, 204, 250–272.
16 S. Hemmatia, A. A. Firooz, A. A. Khodadadi and Y. Mortazavic, Sens. Actuators B, 2011, 160, 1298-1303.
17 C. Zhao, W. Hu, Z. Zhang, J. Zhou, X. Pan and E. Xie, Sens. Actuators B, 2014, 195, 486–493.
18 A. Kusior, J. Klich-Kafel, A. Trenczek-Zajac, K. Swierczek, M. Radecka and K.Zakrzewska, J. Eur. Ceram. Soc., 2013,33,2285-2290
19 G. N. Gerasimov, V. F. Gromov and L. I. Trakhtenberg etc, Russ. J. Phys. Chem., 2014, 88, 503-508.
20 J. Zhao, M. Zheng, X. Lai, H. Lu, N. Li, Z. Ling and J. Cao, Mater. Lett., 2012, 75, 126-129.
21 X. Xu, D. Wang, J. Liu, P. Sun, Y. Guan ,H. Zhang, Y. Sun, F. Liu, X. Liang , Yuan Gao and G. Lu, Sens. Actuators B, 2013, 185, 32-38.
22 P. Song, D. Han, H. Zhang, J. Li, Z. Yang and Q. Wang, Sens. Actuators B, 2014, 196, 434-439.
23 X. Wang, S. Qiu, J. Liu, C. He, G. Lu and W .Liu, Eur. J. Inorg. Chem., 2014,5, 863-869.
24 J. T. McCue and J. Y. Ying, Chem. Mater., 2007, 19, 1009-1015.
25 H. Yang, X. Zhang and A. Tang, Nanotechnology, 2006, 17, 2860-2864.
26 X. Xu, D. Wang, W. Wang, P. Sun, J. Ma, X. Liang, Y. Sun, Y. Ma and G. Lu, Sens. Actuators B, 2012, 171, 1066-1072.
27 P. Sun, X. Zhou, C. Wang, B. Wang, X. Xu and G. Lu. Sens. Actuators B, 2014, 190, 32-39.
28 G. Lu, J. Xu, J. Sun, Y. Yu, Y. Zhang and F. Liu, Sens. Actuators B, 2012, 162, 82-88.
29 J. Sun, J. Xu, Y. Yu, P. Sun, F. Liu and G. Lu, Sens. Actuators B, 2012, 169, 291-296.
30 Q. Qi, P. Wang, J. Zhao, L. Feng, L. Zhou, R. Xuan, Y. Liu and G. Li, Sens. Actuators B, 2014, 194, 440-446.
31 P. Song, D. Han, H. Zhang, J. Li, Z. Yang and Q. Wang, Sens. Actuators B, 2014, 196, 434-439.
32 H. Yang, X. Zhang and A. Tang, Nanotechnology, 2006, 17, 2860-2864.
33 X. Yang, Z. Li, G. Liu, J. Xing, C. Sun, H. Yang and C. Li, CrystEngComm, 2011, 13, 1378-1383.
34 T. Jinkawa, G. Sakai, J. Tamaki, N. Miura and N. Yamazoe, J. Mol. Catal. A: Chem., 2000, 155, 193-200.
35 W. Li, S. Ma and Y. Li., Sens. Actuators B, 2015, 211, 392-402.
36 S. Yan and Q. Wu, Sens. Actuators B, 2014, 205, 329-337.